Edge dislocation mobilities in bcc Fe obtained by molecular dynamics

S. Queyreau,[1,*] J. Marian,[1] M. R. Gilbert,[2] and B. D. Wirth[3,4]

[1]*Lawrence Livermore National Laboratory, P. O. Box 808, Livermore, California 94551, USA*

[2]*EURATOM/CCFE Fusion Association, Culham Science Centre, Abingdon, OX14 3DB, United Kingdom*

[3]*Nuclear Engineering Department, University of Tennessee, Knoxville, Tennessee 37996, USA*

[4]*Department of Nuclear Engineering, University of California at Berkeley, Etcheverry Hall, Berkeley, California 94720, USA*

(Received 17 February 2011; revised manuscript received 5 May 2011; published 18 August 2011)

In the traditional picture of plasticity in bcc metals, edge dislocations have been assumed to play a minor role due to their high mobility with respect to screw dislocations, which then control plastic flow. $\frac{1}{2}\langle 111\rangle\{110\}$ edge dislocations indeed fit this description, as it has been shown by way of numerous atomistic simulations. However, $\frac{1}{2}\langle 111\rangle\{112\}$ edge dislocations have been comparatively much less studied. The recent discovery of a possible regime where they move slowly via thermally activated kink-pair nucleation may have implications in the plastic behavior of bcc materials. Because dislocation mobilities are very difficult to measure experimentally, in this paper, we provide comprehensive mobility laws for both types of edge dislocations as a function of temperature and stress using molecular dynamics simulations. Our results confirm the existence of clearly delimited thermally activated and phonon drag dynamic regimes for $\frac{1}{2}\langle 111\rangle\{112\}$ edge dislocations and of a single viscous drag regime for their $\frac{1}{2}\langle 111\rangle\{110\}$ counterparts. We also provide an analysis to relate the difference in mobility to the dislocation core properties. Our fitted mobility laws may be used in dislocation dynamics simulations of plastic flow involving millions of segments.

DOI: 10.1103/PhysRevB.84.064106 PACS number(s): 61.72.Hh, 31.15.xv

I. INTRODUCTION

The low-temperature behavior of body-centered-cubic (bcc) metals is mainly controlled by the high lattice friction experienced by dislocations. In this regime, it is typically assumed that edge dislocations still move very rapidly and, thus, the rate-controlling plastic mechanism is the thermally activated motion of screw dislocations. Despite an extensive literature on the subject (see reviews in, e.g., Refs. 1 and 2), several questions remain. For example, the nature of anomalous slip in many bcc metals,[3] the disparity between calculated Peierls stresses and measured yield stresses,[4] or the role of nonglide stresses[5] and nonscrew dislocations.

In bcc Fe, slip is known to occur mainly on {110} and {112} planes.[6–8] Activation of one or the other depends not only on the loading orientation, but also on the critical glide stress and the kink formation energy in each family of planes.[9] This is especially true when dislocations move by thermally activated nucleation and propagation of double kinks, where the lattice friction and kink energies on {110} and {112} planes may be very different. In most bcc systems, both of these magnitudes are lower on {110} planes and, indeed, there is ample experimental evidence that {110} slip is preferentially observed at low temperature,[8] whereas {112} glide is only activated at higher temperatures.

As mentioned above, in the traditional picture of bcc slip, it is always assumed that edge dislocations are of the type $\frac{1}{2}\langle 111\rangle\{110\}$ and that their motion is fast and nucleation of kinks is athermal. These features have been confirmed in atomistic simulations for a number of bcc materials.[10–12] In contrast, very little work has been done on edge dislocations of the $\frac{1}{2}\langle 111\rangle\{112\}$ type.[13–15] Recently, Monnet and Terentyev[16] have shown, using molecular dynamics (MD), that the mobility of $\frac{1}{2}\langle 111\rangle\{112\}$ edges in bcc Fe requires a nonzero critical stress to move and that motion proceeds via a displacement mechanism similar to the double-kink formation observed for screw dislocations.

Despite the many physical insights provided in Ref. 16, a fully characterized mobility function covering the entire temperature and stress ranges for $\frac{1}{2}\langle 111\rangle\{112\}$ edge dislocation is still lacking. These functions are of interest to parametrize dislocation dynamics (DD) simulations of complex dislocation microstructures involving large numbers of discrete segments.[17–19] Obtaining mobility functions directly from experimental data is difficult, with only a few studies performed for Fe.[20] In a recent work, Caillard[21,22] has investigated the motion of isolated screw dislocations gliding on {110} planes using *in situ* transmission electron microscopy (TEM) and has obtained velocities related to local stress seen by the dislocation as estimated from its curvature. Even though this represents a tremendous advance in terms of single dislocation mobility measurements, to the authors' knowledge, no such work exists for glide on {112} planes.

The purpose of this paper is to obtain a closed-form mobility function for edge dislocations of the two types in bcc Fe. First, the simulation conditions are presented in detail. Subsequently, we verify the results against the work of Osetsky *et al.*[12] for $\frac{1}{2}\langle 111\rangle\{110\}$ edge dislocations and Monnet and Terentyev for $\frac{1}{2}\langle 111\rangle\{112\}$ dislocations.[16] Finally, we fit the results and the corresponding mobility laws are presented.

II. METHODOLOGY

Our simulations adopt the same configurations proposed by Osetsky and Bacon[12] for $\frac{1}{2}\langle 111\rangle\{110\}$ edge dislocations. A perfect edge dislocation is created along the y axis in the center of an orthorhombic box, as shown in Fig. 1. The z axis coincides with the normal to the glide plane, which can be either of $\langle 110\rangle$ or $\langle 112\rangle$ type. The x axis represents the $\langle 111\rangle$ direction in both cases. Periodic boundary conditions (PBC)

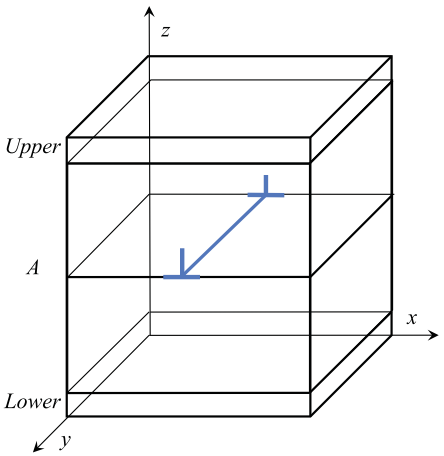

FIG. 1. (Color online) Simulation configuration used to investigate the motion of edges. The dislocation is generated in the middle of the simulation box and can belong to a {110} or a {112} slip plane.

are applied along the line direction y in order to investigate the mobility of an infinitely straight dislocation. Periodicity is also applied along the shear direction x. The volume is divided into three regions. The inner region contains all mobile atoms, and the upper and lower regions contain several layers of atoms in the z direction and are used to apply a pure shear strain or shear stress, depending on the desired type of loading control. The two $\pm z$ faces are therefore necessarily free surfaces.

As discussed in Refs. 12 and 23, the use of periodic boundary conditions along the x axis is associated to the existence of a stress field due to the image dislocation in the periodic cell. However, the image stresses from the replica on the left and the one on the right are of opposite signs and the net shear stress on the simulated dislocation should be zero. We therefore performed preliminary tests to ascertain that the simulation size does not affect the displacement mechanisms or the mobility of edge dislocations. Consequently, the dimensions of the region A are the following at 0 K: $L_x = 29.7$ nm ($\approx 120b$), $L_y = 20.2$ nm ($\approx 80b$), and $L_z = 28.2$ nm ($\approx 114b$). These dimensions account for approximately 1.5 million mobile atoms.

Our calculations are performed using the parallel MD code LAMMPS (Ref. 24) using the Fe potential developed by Mendelev *et al.*,[25] which correctly produces the compact core of screw dislocations.[26–28] All simulations are run in the microcanonical ensemble NVE, where the total number of atoms N, the volume V, and the total energy E of the system are conserved. As in recent calculations,[12] different time-step values are used in our simulations: 5, 2.5, and 1 fs for temperatures of, respectively, 100 K, 200 K, and all other temperatures. As in other recent works,[12,23,29] both stress- and strain-controlled loading conditions are used in this investigation.

Finally, the identification of the dislocation core is performed using a centrosymmetry deviation criterion. Among the different approaches tested,[30,31] the standardized factor proposed by Li[32] is the most efficient in removing thermal vibrations in the specific configurations and temperature range explored here. This procedure is applied every 1000 time steps except at low temperatures, for which this is done more often. The instantaneous and the average dislocation velocities are then calculated by averaging the core displacements along the dislocation line.

III. RESULTS

A. Mobility of edge dislocations on (110) planes

Both strain-[16,23] and stress-controlled[12,23] loading conditions have been employed in previous studies, and here we have performed a set of test simulations using both to confirm that the results were indeed independent of the boundary condition used for $\frac{1}{2}\langle 111\rangle\{110\}$ edge dislocations. After ascertaining this fact, we have chosen to use stress-controlled boundary conditions for the production runs mainly because the stress fluctuations inside the computational cell appear to be smaller than those for strain-controlled conditions. In addition, stress-controlled simulations provide dislocation velocities that are not tied to any one strain rate in particular, as dislocation velocity calculations under these conditions are independent of the box size employed. Strain rate control, however, remains closer to experimental conditions and is therefore more suitable for the strengthening calculations due to nanometric obstacles such as second-phase particles or irradiation defects.[33]

Recent atomistic investigations[10,14] have shown that $\frac{1}{2}\langle 111\rangle\{110\}$ edge dislocations move by generation and propagation of kinks. However, kink energies are very low and, at the temperatures and stresses employed here, the dislocations move rigidly and exhibit a dynamic behavior consistent with a phonon drag mechanism. Indeed, our calculations shown in Fig. 2 indicate that the dislocation moves even at stresses as low as 1 MPa at 100 K. For all practical purposes, this implies the existence of no threshold glide stress. The mobility is linear with the applied stress and inversely proportional to temperature, which is the signature of phonon drag dynamics.[34] The present results are in good qualitative

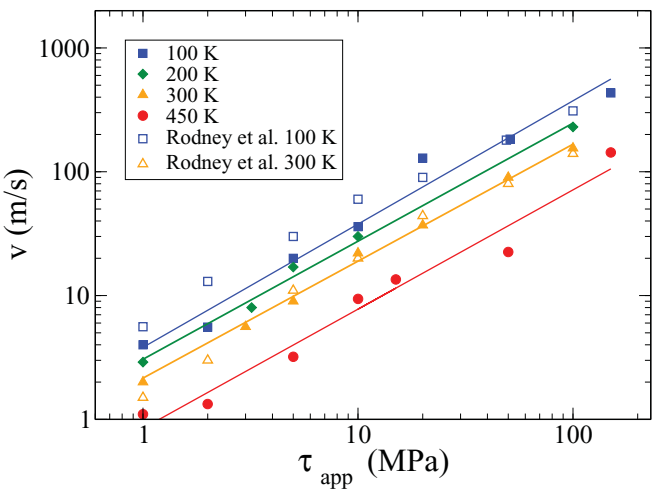

FIG. 2. (Color online) Mobility of a $\frac{1}{2}\langle 111\rangle\{110\}$ edge dislocation in Fe for different applied shear stresses and temperatures. Our results are represented by solid circles, whereas the results obtained by Rodney *et al.* (Ref. 23) are shown as open diamonds. Results are color coded according to the simulation temperature.

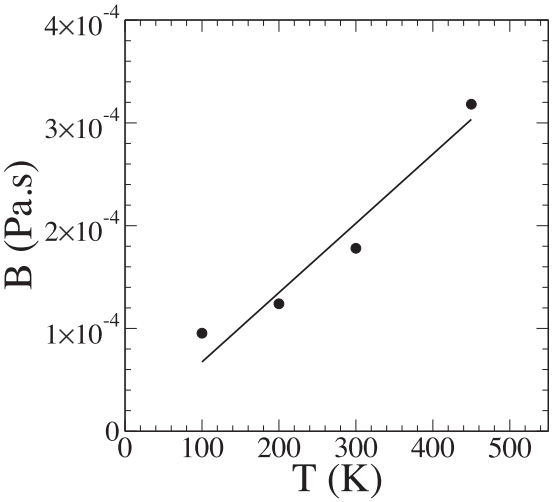

FIG. 3. Temperature dependence of the viscous coefficient appearing in the linear mobility law of the edges.

and quantitative agreement with those reported by Rodney *et al*. at 100 and 300 K.[23]

In the spirit of viscous damping dynamics, we write the mobility of $\frac{1}{2}\langle 111\rangle\{110\}$ edge dislocations as

$$v_{(110)} = \frac{\tau b}{B(T)}, \tag{1}$$

where b is the Burgers vector magnitude and B is the temperature-dependent damping coefficient. B can therefore be obtained as the slope of linear fits to each of the mobility curves in Fig. 2 at each temperature. As shown in Fig. 3, B increases linearly with temperature, and its value approximately triples between 100 and 450 K. From the figure, we obtain $B(T) = 6.7 \times 10^{-7} T$ (Pa s). A similar temperature dependence of B has also been observed by Rong *et al*.[35] using the Fe potential developed by Ackland *et al*.[36] The final numerical expression for the mobility law for $\frac{1}{2}\langle 111\rangle\{110\}$ edge dislocations is therefore

$$v_{(110)} = 370.1 \frac{\tau}{T}, \tag{2}$$

which gives the velocities in m s^{-1} when τ is in MPa and T in K.

B. Mobility of edge dislocations on (112) planes

1. Simulation results

Several time-displacement curves for a $\frac{1}{2}\langle 111\rangle\{112\}$ edge dislocation at 200 K and different applied stresses are shown in Fig. 4. Velocities can be readily extracted from linear fits to these curves. We have systematically obtained dislocation velocities in this fashion for 50, 100, 200, and 300 K and stresses ranging from 1 to 1000 MPa. The results are given in logarithmic scale in Fig. 5.

Two regimes can clearly be distinguished at each temperature. The dislocation velocity first grows exponentially until transitioning to a more standard linear regime. The transition stress decreases with temperature, which is a telltale sign of a thermally activated mechanism of motion. After this stress is reached, the mechanism of motion shifts to viscous damping dynamics. Above the transition stress, the velocities of $\frac{1}{2}\langle 111\rangle\{112\}$ edge dislocations are reasonably similar to their $\frac{1}{2}\langle 111\rangle\{110\}$ counterparts. However, at low stresses (and low temperatures), edge dislocation glide on (112) planes is considerably slower. As first observed by Monnet and Terentyev,[16] the velocity response displays a directional asymmetry on the (112) plane corresponding to the twinning-antitwinning (TD-AT) asymmetry.

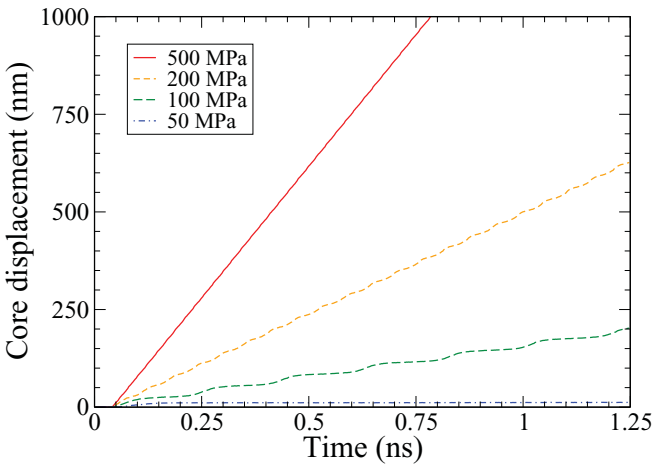

FIG. 4. (Color online) Time-displacement curve for an edge dislocation gliding on a {112} plane at 200 K and different applied stresses.

2. Kink structure and analysis

To further characterize the mechanism of motion in the thermally activated regime, we have performed a careful analysis of the core configuration as a function of time. Results for a dislocation at 50 K and 300 MPa of applied stress in the twinning direction are shown in Fig. 6. The figure shows a sequence of core configurations taken at intervals of 0.5 ps, where episodes of double-kink nucleation and propagation can be clearly recognized. Over 15 ps, the dislocation moved a total distance of $3b$, which corresponds to a velocity of

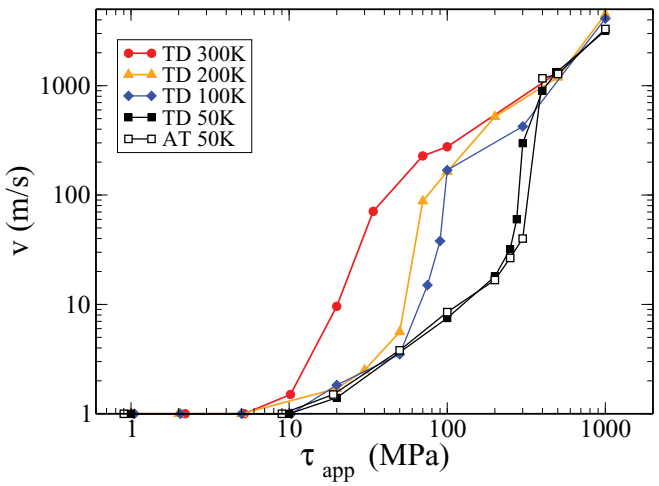

FIG. 5. (Color online) Edge dislocation velocities on (112) planes as a function of the applied stress and temperature. TD represents twinning direction, while AT indicates antitwinning sense.

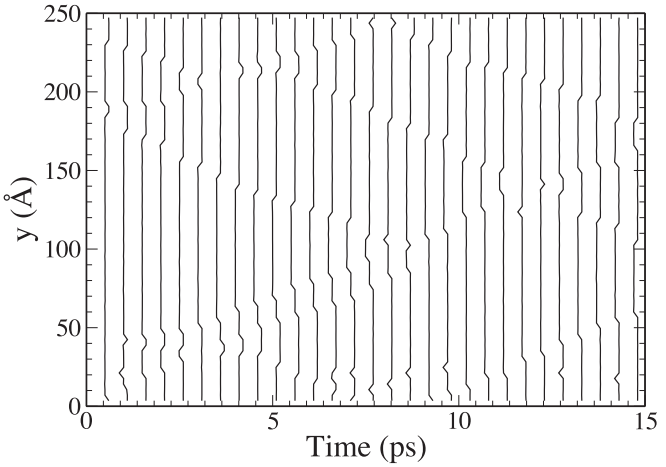

FIG. 6. Core configurations of a $\frac{1}{2}\langle 111\rangle\{112\}$ edge dislocation at 50 K and under a constant stress of 300 MPa moving in the antitwinning sense. Double-kink nucleation and motion can be clearly recognized.

$\approx$50 m s^{-1}. Our analysis is in agreement with that of Monnet and Terentyev,[16] who observed the same kink-pair nucleation and propagation sequences.

Double kinks are essentially the end points of finite portions of dislocation line that jump across a relatively stiff energy barrier from one equilibrium configuration to the next. To study kink structure and characterize the transition path, we have generated atomistic configurations of left- and right-handed kinks and have measured their respective energies. The relaxed configurations for a kink pair in a dislocation dipole are shown in Fig. 7. The structures showcase the planar nature of the dislocation core, which spans several {111} planes. The energy of this double kink is 0.15 eV, which is higher than the value of 0.08 eV calculated by Li-Qun *et al.*,[14] but still sufficiently low (certainly compared to screw dislocations) to allow $\frac{1}{2}\langle 111\rangle\{112\}$ edge dislocations to reach their viscous drag dynamic regime at low stresses and relatively low temperatures.

In addition, we have characterized the energy path attendant to kink nucleation using the nudged elastic band (NEB) method.[37] The results are shown in Fig. 8, where two distinct energy states can be observed. Much akin to the manner of screw dislocations, these correspond to "easy" and "hard" core configurations, although, as the figure shows, the energy difference of 0.08 eV is very low and this effect is likely to play no role at finite temperature. Thus, the periodicity of easy (or hard) cores along the $\langle 111\rangle$ direction is $2b$. In the dislocation motion sequence shown in Fig. 6, it appears that double kinks are produced easier and in more abundance from some configurations than others. At 50 K, this may well be a manifestation of the existence of hard and easy cores, which have slightly different energy barriers for kink pair nucleation. This effect is expected to be smeared out by thermal fluctuations at higher temperatures.

To further explore the difference between these two nondegenerate core structures, we have calculated the core disregistry in both cases and, from it, the Burgers vector density as a function of distance from the dislocation core.[38] Figure 9 shows that the difference between both easy and hard configurations is very subtle and, in fact, only appreciable at the point of maximum Burgers vector density. The overall shape of the curves is in good agreement with those published by Monnet and Terentyev.[16] We conclude that this effect is indeed negligible on the dynamics of the dislocations at temperatures larger than 50 K.

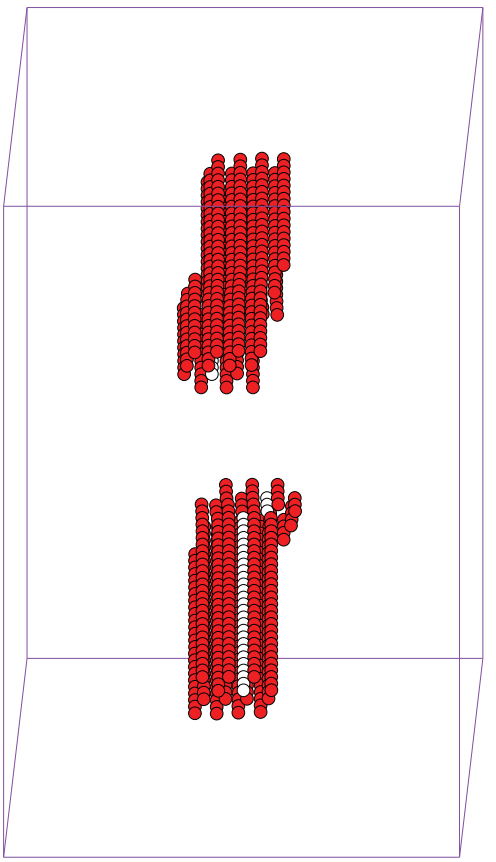

FIG. 7. (Color online) Atomistic structure of two single kinks in a $\frac{1}{2}\langle 111\rangle\{112\}$ edge dislocation. The energy of one kink is 0.075 MeV.

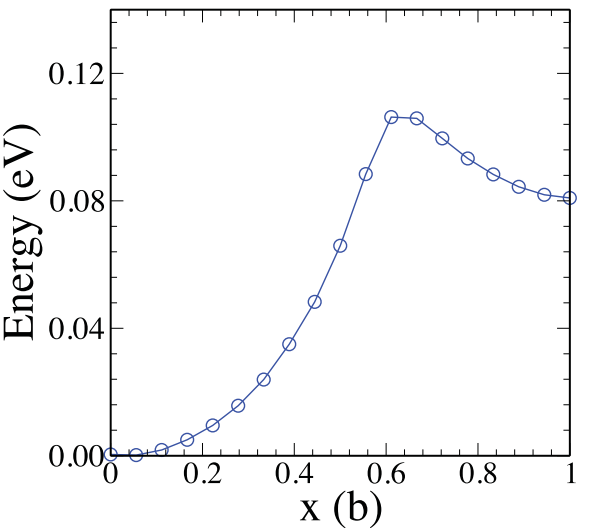

FIG. 8. (Color online) Minimum energy path (Peierls energy) for a rigid $\frac{1}{2}\langle 111\rangle\{112\}$ edge dislocation along the $\langle 111\rangle$ in the twinning sense.

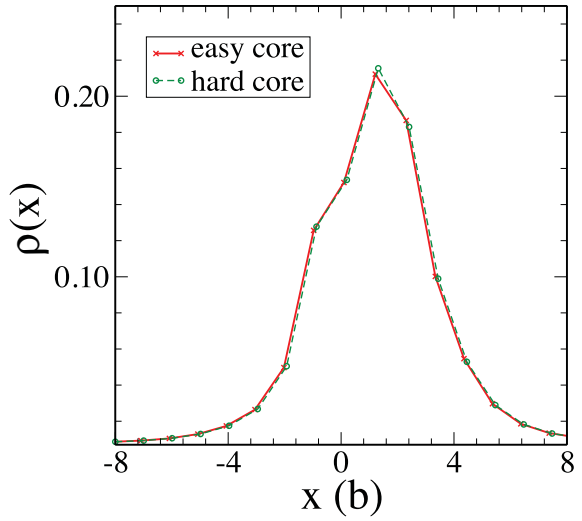

FIG. 9. (Color online) Density of Burgers vector calculated as in Ref. 38. An asymmetry can be recognized in the shape of $\rho(x)$.

What is not negligible, however, is the threshold stress (akin to the Peierls stress for screw dislocations) required for the dislocation to move in the twinning and antitwinning directions. Using the same methodology as in Refs. 39 and 40, the Peierls stress along TD is of 260 ± 10 MPa, while along AT it is 520 ± 10 MPa. These values are significantly smaller than the Peierls stresses for screw dislocations in Fe, but, here too, the antitwinning stress is approximately twice the value of the twinning stress. These values mark the zero-temperature transition between the thermally activated and phonon drag regimes. As we have pointed out earlier, the actual threshold stresses at different temperatures are noticeably smaller. Next, we analyze the data presented in Fig. 5 and obtain a stress and temperature-dependent mobility law.

3. *Fitting of the mobility function*

In the low-stress regime controlled by the thermally activated nucleation of kinks, we use the phenomenological mobility law proposed originally for screw dislocations[41,42]:

$$v_{(112)} = \frac{A\tau_n}{k_B T} \exp\left(-\frac{\Delta H(\tau_n)}{k_B T}\right), \tag{3}$$

where k_B is Boltzmann's constant and A is a fitting constant that accounts for various effects such as the attempt frequency, kink width, dislocation line length, etc. τ_n is a normalized stress $\tau_n = \tau_a/\tau_d$ where τ_a and τ_d are, respectively, the applied and temperature-dependent transition stresses. τ_d is obtained directly from the MD results in Fig. 5 and its values are given in Table I. Only the TD data have been fitted.

We have checked the dependence of the dislocation velocity with the dislocation length by varying the y dimension in Fig. 1 in a set of simulations at 50 K from 12 to 120 nm. For all cases, the resulting velocity was found to be constant, which we attribute to the fact that, once the dislocation line surpasses the critical length for stable double-kink nucleation (here smaller than 12 nm), the mobility is independent of the dislocation length and kink nucleations can be considered as uncorrelated events.

TABLE I. Values of the transition stress τ_d between the thermally activated and the linear regimes, estimated from the MD simulations.

T (K)	50	100	200	300
τ_d (MPa)	300	100	75	30
B ($\times 10^{-5}$ Pa s)	4.5	17.0	11.3	9.4

As discussed in detail by Kocks, Argon, and Ashby,[41] the activation free enthalpy ΔH is a decreasing function of the applied stress. They proposed the following generic form:

$$\Delta H(\tau_a) = \Delta H_0\left(1 - \tau_n^p\right)^q, \tag{4}$$

where ΔH_0 is the zero-stress activation energy. This key quantity can be calculated by molecular statics calculations as the sum of the formation energy of two single, opposite kinks.[43] From the results of the previous section, here we use a value of 0.15 eV, significantly smaller than for screws (0.67 eV).[43] For isotropic linear elasticity, $p = 0.5$ and $q = 1.25$. Here, however, we leave them also as fitting parameters to account for nonlinear, nonelastic, and anisotropic effects found in MD simulations. The fit consisting of Eqs. (3) and (4) does not take into account backward jumps and provides no physical insight about the shape of ΔH at intermediate stresses. The values for p and q provide the asymptotic behavior of ΔH at very low stresses and close to the Peierls stress, respectively. However, in between, only phenomenological assumptions can be made, of which Eq. (4) is the most widely used.

Using Eqs. (3) and (4) and the transition stresses in Table I, we perform a least-squares fit to the data corresponding to simulations along the twinning sense in Fig. 5 and obtain values of $A = 1.45$ m/eV s^{-1}, $p = 0.13$, and $q = 0.68$. As Fig. 10 shows, the resulting mobility function provides a very good fit for the velocities corresponding to the thermally activated regime, particularly at 50 and 100 K. The overall fitting error is approximately 5%. It is worth mentioning that we have also performed a fit using the thermally activated mobility law used by Naamane *et al.*,[17] which does account for both forward and backward jumps and assumes $p = 0.5$ and $q = 1$. Nevertheless, the resulting fit provides slightly worse agreement with the MD data than the one used here. The final mobility form in numerical form is then

$$v_{(112)} = 1.68 \times 10^4 \frac{\tau_n(T)}{T} \exp\left\{-0.15[1 - \tau_n(T)^{0.13}]^{0.68}\right\}, \tag{5}$$

noting that the normalized stress is temperature dependent according to the values in Table I. The reason why the transition stress at 50 K is larger than at 0 K is not clear, although it may be due to data scatter.

Figure 10 also shows the beginning of the linear fits corresponding to the viscous drag regime. These simply have been obtained as

$$v_{(112)} = \frac{\tau_a b}{B(T)}, \tag{6}$$

and the results are given in Table I. In this case, the phonon drag coefficient does not show a consistent trend with temperature, which may simply be an indication that the phonon drag regime is not fully established within the stress regime

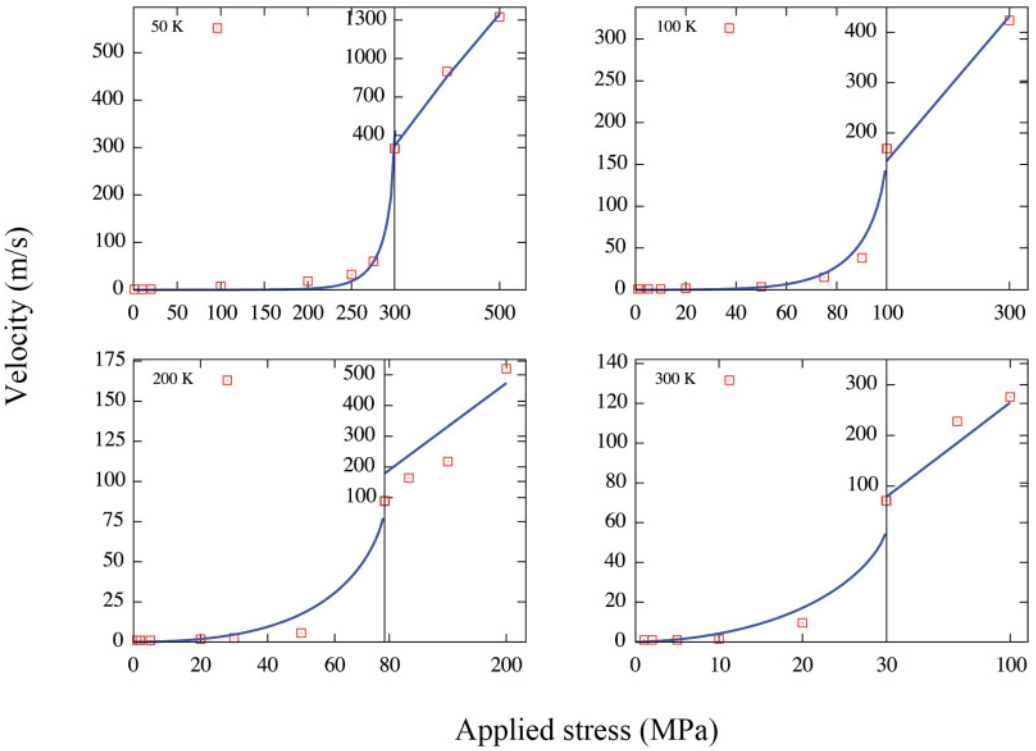

FIG. 10. (Color online) Comparison of the fitted edge mobility in TD (continuous line) using Eqs. (3) and (4) with the MD results in a linear scale (red squares). The thermally activated regime is well captured by the mobility function, especially at low temperature.

explored here. The above equation was fitted without an independent constant, except at 50 K, where one was needed to maintain a reasonable transition stress. For $T = 50$ K, the complete expression is then $v_{\langle 112\rangle} = 5.5\tau_a - 1307.0$, which gives velocities in m s^{-1} when τ_a is in MPa.

For verification, we compare our values with the calculations performed by Monnet and Terentyev[16] using a strain rate-controlled MD simulation. In their calculations, when the edge dislocation moved at an average velocity of 8.4 m s^{-1} at 100 and 50 K, the resulting critical stress was, respectively, of 33 ± 14 and 125 ± 23 MPa. In the present investigation, in order to reach the same velocity, the applied stress must be 63 and 112 MPa for the same temperatures.

IV. DISCUSSION AND CONCLUSIONS

The main findings of this paper can be summarized as follows:

(i) For $\frac{1}{2}\langle 111\rangle\{110\}$ edge dislocations, a linear mobility is obtained consistent with viscous dynamics. The damping coefficient increases linearly with temperature in agreement with phonon drag theory. No threshold stress is required to initiate dislocation motion.

(ii) For $\frac{1}{2}\langle 111\rangle\{112\}$ edge dislocations, two dynamic regimes have been identified. At low applied stress, the dislocation moves by thermally activated nucleation of kink pairs, in agreement with earlier works.[16] The mobility displays the characteristic twinning and antitwinning asymmetry of (112) bcc slip. At higher stresses, a transition to a linear mobility is found, signaling transition from thermally activated to phonon drag dynamics. No dependence upon the dislocation length is found.

(iii) We have identified two stable core energy states: the easy core, being about 0.08 eV more stable than the hard core. No appreciable differences in the atomic disregistry between both cores have been found. In any case, the energy difference between both states is too small to play any role, even at low temperatures.

(iv) The threshold stresses (akin to Peierls stress for screw dislocations) for slip on (112) planes in the TD and AT directions were calculated using molecular statics, and values of 260 and 510 MPa, respectively, were found. These stresses are approximately five times smaller than the Peierls stress for screw dislocations using the same potential.[28] The double-kink formation energy was found to be 0.15 eV, also significantly smaller than for screw dislocations.

(v) Functional mobility laws are provided for each dynamic regime obtained from fitting physically based expressions to the simulation raw data.

The results obtained here for $\frac{1}{2}\langle 111\rangle\{110\}$ edge dislocations are in agreement with previous calculations and fit to the traditional idea of bcc plasticity governed by screw dislocations. $\frac{1}{2}\langle 111\rangle\{112\}$ edges deviate from this idea in the sense that they may have slow mobility owing to their thermally activated behavior in the proper stress and temperature regimes. How these mobilities impact the overall yield and flow strength of bcc Fe at low temperatures is not immediately clear. DD calculations should be performed under conditions of {112}

slip to quantify this effect. In this sense, a $\frac{1}{2}\langle 111\rangle\{112\}$ screw dislocation mobility will be provided in a forthcoming publication so that both types of dislocation populations can be evolved concurrently. In addition, these mobilities are useful to assess the temperature dependence of phenomena such as precipitation or irradiation hardening, where dislocation glide is hampered by obstacles. Again, our results should be seen as useful and necessary input to calculations based on line tension models or dislocation dynamics of large dislocation ensembles.

ACKNOWLEDGMENTS

This work was performed under the auspices of the U S Department of Energy by Lawrence Livermore National Laboratory under Contract No. DE-AC52-07NA27344. We specifically acknowledge support from the Laboratory Directed Research and Development Program under Project No. 09-SI-003. This work was partly funded by the RCUK Energy Programme under Grant No. EP/I501045 and the European Communities under the contract of Association between EURATOM and CCFE.

*queyreau1@llnl.gov

[1] L. Kubin, in *Reviews on the Deformation Behavior of Materials*, edited by P. Feltham (Freund, Tel Aviv, 1982), Vol. 4(3), p. 181.

[2] J. W. Christian, Metall. Trans. **36**, 29 (1983).

[3] R. Gröger, A. G. Bailey, and V. Vitek, Acta Mater. **56**, 5401 (2008).

[4] R. Gröger, A. G. Bailey, and V. Vitek, Philos. Mag. Lett. **87**, 113 (2007).

[5] V. Vitek, M. Mrovec, and J. L. Bassani, Mater. Sci. Eng., A **365**, 31 (2004).

[6] W. A. Spitzig and A. S. Keh, Acta Metall. **18**, 611 (1970).

[7] P. Franciosi, Acta Metall. **31**, 1331 (1983).

[8] T. Taoka, S. Takeuchi, and E. Furubayashi, J. Phys. Soc. Jpn. **19**, 353 (1964).

[9] A. J. Opinsky and R. Smoluchowski, J. Appl. Phys. **22**, 1380 (1951).

[10] J. Chang, V. V. Bulatov, and S. Yip, J. Comput.-Aided Mater. Des. **6**, 165 (1999).

[11] J. Chang, W. Cai, V. V. Bulatov, and S. Yip, Comput. Mater. Sci. **23**, 111 (2002).

[12] Y. N. Osetsky and D. J. Bacon, Modell. Simul. Mater. Sci. Eng. **11**, 427 (2003).

[13] M. Yamaguchi and V. Vitek, J. Phys. F: Met. Phys. **5**, 1 (1975).

[14] C. Li-Qun, W. C. Yu, and Y. Tao, Chin. Phys. B **17**, 662 (2008).

[15] S. Yu, C.-Y. Wang, and Y. Yu, Solid State Sci. **11**, 733 (2009).

[16] G. Monnet and D. Terentiev, Acta Mater. **57**, 1416 (2009).

[17] S. Naamane, G. Monnet, and B. Devincre, Int. J. Plast. **26**, 84 (2009).

[18] G. Monnet, S. Naamane, and B. Devincre, Acta Mater. **59**, 451 (2011).

[19] S. Queyreau, G. Monnet, and B. Devincre, Acta Mater. **58**, 5586 (2010).

[20] L. P. Kubin and F. Louchet, Acta Metall. **27**, 337 (1979).

[21] D. Caillard, Acta Mater. **58**, 3493 (2010).

[22] D. Caillard, Acta Mater. **58**, 3504 (2010).

[23] D. J. Bacon, Y. N. Osetsky, and D. Rodney, in *Dislocations in Solids*, edited by J. P. Hirth and L. Kubin (Elsevier, Amsterdam, 2009), Vol. 15, Chap. 88, p. 14.

[24] [http://lammps.sandia.gov].

[25] M. I. Mendelev, S. Han, D. J. Srolovitz, G. J. Ackland, D. Y. Sunand, and M. Asta, Philos. Mag. **83**, 3977 (2003).

[26] S. L. Frederiksen and K. W. Jacobsen, Philos. Mag. **83**, 365 (2003).

[27] C. Domain and G. Monnet, Phys. Rev. Lett. **95**, 215506 (2005).

[28] J. Chaussidon, M. Fivel, and D. Rodney, Acta Mater. **54**, 3407 (2006).

[29] D. Rodney, Phys. Rev. B **76**, 144108 (2007).

[30] C. L. Kelchner, S. J. Plimpton, and J. C. Hamilton, Phys. Rev. B **58**, 11085 (1998).

[31] G. J. Ackland and A. P. Jones, Phys. Rev. B **73**, 054104 (2006).

[32] J. Li (2003) [http://mt.seas.upenn.edu/Archive/Graphics/A/].

[33] Y. N. Osetsky, D. J. Bacon, and V. Mohles, Philos. Mag. **83**, 3623 (2003).

[34] VI.. Alshits and V. L. Indenbom, in *Dislocations in Solids*, edited by F. R. N. Nabarro and J. P. Hirth (Elsevier, Amsterdam, 1986), Vol. 7, p. 43.

[35] Z. Rong, Y. N. Osetsky, and D. J. Bacon, Philos. Mag. **85**, 1473 (2005).

[36] G. J. Ackland, D. J. Bacon, A. F. Calder, and T. Harry, Philos. Mag. A **75**, 713 (1997).

[37] D. Sheppard, R. Terrell, and G. Henkelman, J. Chem. Phys. **128**, 134106 (2008).

[38] M. Yamaguchi and V. Vitek, J. Phys. F **5**, 11 (1975).

[39] J. Li, C.-Z. Wang, J.-P. Chang, W. Cai, V. V. Bulatov, K.-M. Ho, and S. Yip, Phys. Rev. B **70**, 104113 (2004).

[40] G. Wang, A. Strachan, T. Cajin, and W. A. Goddard III, Modell. Simul. Mater. Sci. Eng. **12**, S371 (2004).

[41] U. K. Kocks, A. S. Argon, and M. F. Asby, Prog. Mater. Sci. **19**, 1 (1975).

[42] J. P. Hirth and J. Lothe, *Theory of Dislocations* (Krieger, 1992).

[43] L. Ventelon, F. Willaime, and P. Leyronnas, J. Nucl. Mater. **386**, 26 (2009).